Improved emission uniformity from a liquid-jet laser-plasma extreme-ultraviolet source

Björn A. M. Hansson, Sofia Mosesson, and Hans M. Hertz

Many modern compact soft-x-ray and extreme-ultraviolet (EUV) imaging systems operate with small fields of view and therefore benefit from the use of small high-brightness sources. Such systems include water-window microscopes and EUV lithography tools. We show that the photon losses in such systems can be minimized while uniformity of object-plane illumination is maintained by controlled scanning of the source. The improved collection efficiency is demonstrated both theoretically and experimentally for a scanned laser-plasma source compared with static sources. A prospective aerial image microscope and a liquid-xenon-jet laser-plasma source are offered as examples of modern imaging tools that may benefit from such scanning of the source. © 2004 Optical Society of America

OCIS codes: 110.3960, 340.7440, 340.7460.

1. Introduction

A growing number of soft-x-ray and extreme-ultraviolet (EUV) imaging systems based on compact plasma sources are being achieved today. Two examples of such systems are water-window x-ray microscopes[1,2] and tools for EUV lithography (EUVL).[3–5] Unfortunately, the limited power available from existing compact EUV and soft-x-ray sources still limits the performance of these tools. However, several of these systems have relatively small fields of view and therefore benefit from small, high-brightness laser-plasma sources for photon economy. In the present paper we demonstrate how scanning of a small source can minimize photon losses while maintaining object-plane illumination uniformity.

Although synchrotron sources are well suited for small-field applications because of their high brightness, they are impractical for applications for which it is desired to integrate a tool into an existing facility. Examples include tools for EUVL to be introduced into modern integrated-circuit and mask development facilities, and soft-x-ray microscopy that would strongly benefit from being available in the small-scale laboratory.

High-power compact sources for the soft-x-ray–EUV wavelength range are divided into two major groups: gas discharges and laser plasmas. The performances of both have increased significantly over the past few years, driven by the demand for EUVL. The current status of both gas-discharge and laser plasma sources for EUVL is described in Ref. 6. The gas-discharge plasmas (e.g., *z*-pinch, hollow-cathode, dense plasma focus) are characterized by large source sizes,[7] FWHM > 380 μm, and availability of high average power[8] up to 150 W/(2% bandwidth 2πsr) in short bursts. The laser plasmas are typically operated either with gas–cluster–spray targets or liquid-jet–droplet targets. The gas–cluster–spray results in a fairly large source,[9] FWHM > 100 μm, whereas the liquid jet or droplets can result in a small-diameter source,[10] FWHM > 20 μm, with high brightness. Laser plasmas have, however, so far reached lower powers than discharge plasmas,[11] up to 22 W/(2% bandwidth 2πsr). Although the discussion above has covered compact sources for EUVL, both laser plasmas and gas-discharge plasmas can generate soft x rays for, e.g., microscopy.[1,12]

Soft-x-ray microscopes and EUVL tools follow the same optical arrangement as their visible-light counterparts. Collector–illuminator optics transfer radiation from the source to the object (specimen or lithographic mask), and an objective images the ob-

When this research was conducted, B. A. M. Hansson (bjorn.hansson@biox.kth.se), S. Mosesson, and H. M. Hertz were with Biomedical & X-Ray Physics, Royal Institute of Technology/Albanova, SE-106 91 Stockholm, Sweden. B. A. M. Hansson is now with Cymer, Inc., Cymer, 17075 Thornmint Court, San Diego, California 92127. S. Mosesson is now with Peek Traffic AB, P.O. Box 10158, SE-121 28 Stockholm, Sweden.

Received 18 November 2003; revised manuscript received 28 June 2004; accepted 1 July 2004.

0003-6935/04/295452-06$15.00/0

Table 1. Comparison of Optical Parameters of Small-Field EUV and Soft-X-Ray Imaging Systems and Typical Compact Plasma Sources

Tool or Source Type	Field or Source Size	NA	Étendue (μm^2)
Tool	Field size		
Compact soft-x-ray microscope[a]	25-μm diameter[b]	0.056[b]	4.84
AIM[c]	50 μm × 50 μm[b]	0.0625[b]	30.7
Microexposure tool[d]	0.6 mm × 0.2 mm[e]	0.3[e]	33 928
Source type	Source size		
Laser-plasma source[f]	>20 μm FWHM	1[g]	>986
Discharge-plasma source[h]	>380 μm FWHM	1[g]	>356 292

[a]Ref. 1.
[b]Values refer to the object side.
[c]Ref. 5.
[d]Ref. 4.
[e]Values refer to the image side.
[f]Ref. 10.
[g]The collection is assumed to be limited to a hemisphere.
[h]Ref. 7.

ject to the image plane (detector or resist-coated wafer). Throughout the system the numerical aperture, NA, and the area, A, are coupled through the étendue invariant[13]:

$$\text{étendue} = A\pi(\text{NA})^2 . \quad (1)$$

A and NA can represent the field size and the NA of the objective but also the projected source area and the NA of the collector. If this source–collector étendue is larger than the étendue of the objective, only a fraction of the power emitted from the source is usable. Either the collection angle has to be limited or only a smaller effective area of the source can be collected. Table 1 lists three compact-source-based tools with small fields of view, and two typical sources. The source–collector étendue, assuming a collector an NA of 1, is larger than the étendue of any of the three optical systems except for one, meaning that source power will be lost.

Illumination uniformity and pupil fill is achieved by matching the properties of the source and the illumination optics. Two main methods of illumination are possible (see, e.g., Ref. 14): critical illumination, as illustrated in Fig. 1, for which the source is directly imaged onto the object, and Köhler illumination, for which the source is imaged in the back focal plane of the objective and the collector pupil is instead imaged onto the object. In addition, flys' eyes[13] and ripple plate[14] concepts, e.g., can be applied to manipulate the distribution of illumination. Critical illumination requires only one mirror in its simplest form and is therefore the only possible choice for the soft-x-ray microscope of Table 1 because of the low efficiency of optical components at soft-x-ray wavelengths. The microexposure tool[4] also uses critical illumination because of its simplicity, and in general we consider only critical illumination throughout this paper.

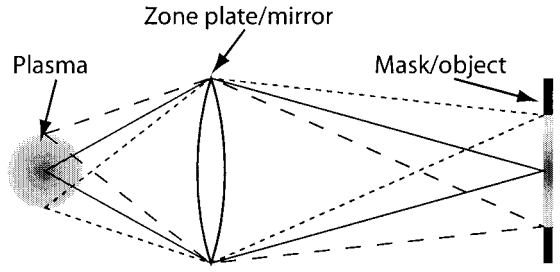

Fig. 1. Illustration of the simplest form of critical illumination in which the source is imaged onto the mask/object by only one optical element. For simplicity, the optical element is illustrated as a lens, but it may equally well be a mirror or a zone plate.

In the present paper we focus on minimizing photon losses while we maintain uniformity of the object's illumination. We report in particular on the way in which a small laser-plasma source can be spatially scanned to improve the integrated illumination uniformity, thus minimizing the required total source power. For clarity, we use aerial image microscope (AIM),[5] which is used to review defects in EUV masks, in combination with a high-brightness liquid-xenon-jet source as examples throughout the paper; naturally, the concept has a more general applicability.

2. Simulation and Discussion

With critical illumination, the source is directly imaged onto the object plane. In a quadratic field of view, as for the AIM tool,[5] it is therefore desired that the source have uniform emission over a square area and that a large fraction of the total power be emitted from within this square. In the following analysis, when we discuss power or brightness we mean in-band power, i.e., radiation within the wavelength range utilized by the optical system. In as much as we use the AIM tool as an example of an optical system, here we mean the useful radiation for EUV lithography applications, i.e., the radiation transmitted by the optical system based on Mo–Si multilayer mirrors, basically a few-percent bandwidth near λ = 13.5 nm, depending on the parameters of the multilayer coating and on the number of mirrors. Fur-

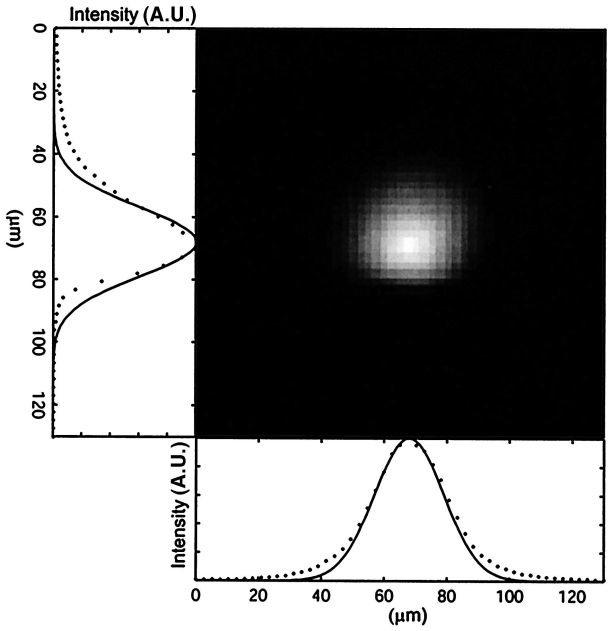

Fig. 2. EUV image of a 26-μm FWHM plasma. Dotted curves, intensities along the x and y axes. Solid curves, Gaussian curves of 26-μm FWHM for comparison.

thermore, for simplicity we assume that the coherency factor[5] is 1: $\sigma = 1$.

Assuming that the source is projected onto a plane normal to the optical axis, the brightness distribution from a plasma source can be modeled by a Gaussian emission profile:

$$B_s(r) = B_0 \exp\left(\frac{-r^2 \ln 2}{r_{1/2}{}^2}\right), \tag{2}$$

where $2r_{1/2}$ is the FWHM size of the plasma. Although the model does not take the three-dimensional nature of the plasma into account, it should still be accurate, at least at smaller collection angles. The validity of assuming that the emission profile is Gaussian is verified in Fig. 2 by comparison of an experimental emission distribution (dotted curves), further discussed below, to the theory according to Eq. (2) (solid curves), and, as can be seen, the model is reasonably correct, at least in one dimension. The deviation in the other dimension occurs because the plasma was imaged at 45° to the axis of symmetry. For such a plasma with a near-Gaussian emission profile, the straightforward way to reach the required brightness-uniformity specification is to increase the total size of the plasma, as illustrated in Fig. 3(a). A centered square area of the source with side lengths l and consequently diagonal $l\sqrt{2}$ will have an emission uniformity of $\pm x\%$ if the FWHM size of the plasma, $2r_{1/2}$, is obtained from

$$(1 - 2x)\, B_0 = B_0 \exp\left[\frac{-(l\sqrt{2})^2 \ln 2}{r_{1/2}{}^2}\right]. \tag{3}$$

It has been shown[10] that it is possible to modify the FWHM source size with a liquid-jet laser-plasma source of 20–250 μm. In that way it would be possible to choose the optimal source size to obtain the specific intensity distribution. However, the technique of increasing only the plasma size is not energy effective because the larger the plasma, the less the total energy collected, owing to the étendue limitation discussed above.

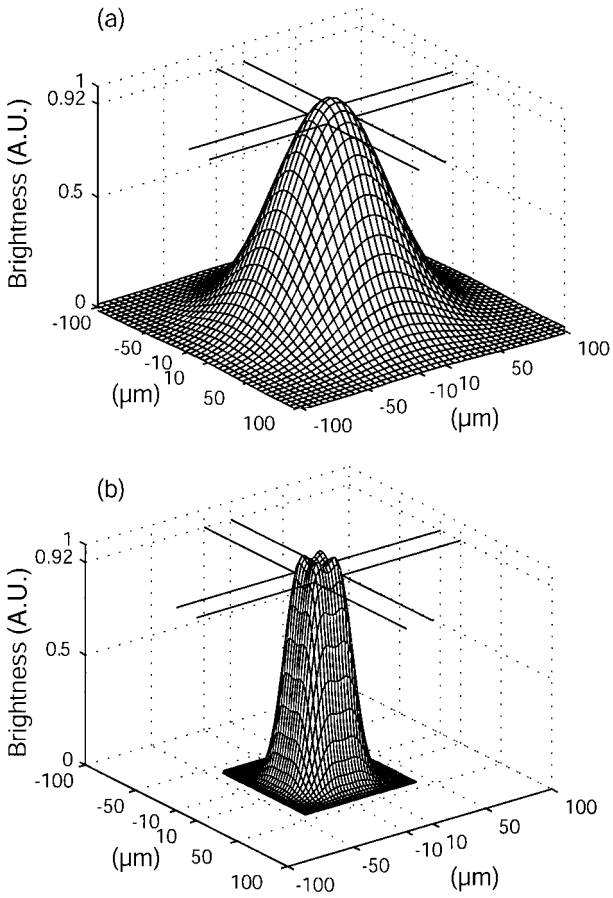

Fig. 3. (a) Simulations of one large single plasma and (b) integrated image of four small plasmas. The emission uniformity is ±4% within a 20 μm × 20 μm square in both figures.

When it is possible to generate a small plasma, and in a situation in which a large number of pulses are needed to reach the required exposure dose, a simple scheme in which the small plasma is moved among four positions, (a, a), $(a, -a)$, $(-a, a)$, and $(-a, -a)$; i.e., the corners of a centrally placed square with side lengths $2a$, can instead be applied. This will generate the following brightness distribution:

$$B_s(x, y) = \frac{B_0}{4} \sum_{i=-1,1} \sum_{j=-1,1} \times \exp\left\{\frac{-[(x + ia)^2 + (y + ja)^2] \ln 2}{r_{1/2}{}^2}\right\}, \tag{4}$$

which will lead to better uniformity distribution over a square area of the source such that a smaller total source size will still meet the uniformity specification.

For example, assume that the specification is to achieve a brightness uniformity of ±4% within a 20 μm × 20 μm square. Instead of reaching this brightness as in Fig. 3(a) by increasing the total size of the plasma to FWHM 81.5 μm, we can achieve it by moving a 20-μm FWHM Gaussian plasma within the four corners of an 18.8 μm × 18.8 μm square, as in Fig. 3(b). Only 5.1% of the total energy will be emitted within the 20 μm × 20 μm square in the first case, compared with 26.6% in the second case, a 5.2× gain in usable source power.

However, the power illuminating the object field is limited also by the available collection angle, and to illustrate further the advantage of scanning a small source we investigated the total power reaching the object field as a function of the source emission profile. This power, P_o, is given by

$$P_o = P_s \, \eta \, T , \tag{5}$$

where P_s is the total power radiated by the source into 2π sr and T is the transmission of the collector–illuminator system, i.e., the integrated reflectivity of its mirrors. The collection efficiency, η, is

$$\eta = \frac{\int_{A_e} B_s \, dA \, \Omega_c}{P_s} , \tag{6}$$

where B_s is the brightness of the source [(W/mm^2)/sr], Ω_c is the solid angle of the collector, and A_e the effective area of the source from which the emission is collected. In analogy with the discussion above, this effective collectable source area, A_e, will be limited by the emission uniformity profile of the source and the desired illumination uniformity. The available collection angle, Ω_c, is then given by the étendue limitations imposed by the object side of the system and A_e through Eq. (1), where $NA = [1 - (1 - \Omega_c/2\pi)^2]^{1/2}$. Thus the numerator in Eq. (6) is the power reaching the collector from the effective collectable area of the source. Angular emission uniformity is assumed.

Figure 4 shows how collection efficiency η, defined in Eq. (6), varies with different parameters for a system that meets the étendue specification of the AIM tool (see Table 1). The collection efficiency is given for collection angles; a smaller collection angle means that a larger source area is collected owing to the conservation of étendue. Furthermore, the collection efficiency is given both for a nonscanned plasma with a Gaussian emission profile [cf. Fig. 3(a)] and for the integrated image of four plasmas [cf. Fig. 3(b)]. For each given collection angle, the size of the single plasma or the distances among the four plasmas are as small as possible to meet three different uniformity specifications (±2.5%, ±5%, and ±10%). A general conclusion from the figure is that larger collection angles will give higher collection efficiency. For the single-plasma case this is obvious because the same fraction of the total source area will be collected, independently of the collection angle, resulting in a collection efficiency that basically is dependent only on the collection angle. For the four-plasma case

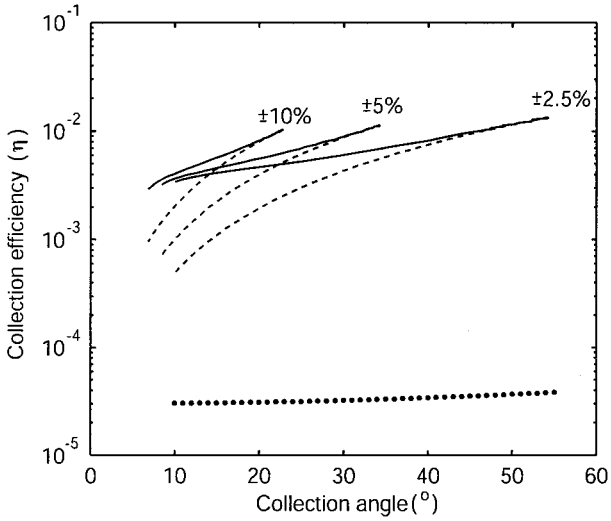

Fig. 4. Collection efficiency η, relative to various parameters for a system meeting the étendue specification of the AIM tool. It is given for both single Gaussian plasmas of various sizes (dashed curves) and for four 20-μm plasmas scanned as described in the text (solid curves), where, at each point, the size of the single plasma or the distances among the four plasmas are as small as possible to meet three different uniformity specifications (±2.5%, ±5%, and ±10%). The collection efficiency of a 380-μm FWHM Gaussian plasma is also illustrated (dotted curve).

the situation is significantly better at small collection angles, where the collected-area fraction becomes larger. At small collection angles our two-dimensional source model should also be most accurate, as discussed above. From a systems perspective, increased performance at smaller collection angles is important because large-angle collectors are costly and their manufacture is difficult. Finally, the collection efficiency of a 380-μm FWHM Gaussian plasma, the size of one of the smallest discharge plasmas,[7] is also illustrated in Fig. 4 (dotted curve). It should, however, be noted that the uniformity is better than ±2.5% for that case because uniformity is not the limiting factor for such a large plasma.

3. Experiment and Discussion

To show the feasibility of the four-plasma scheme, we performed a proof-of-principle experiment. The experimental arrangement is illustrated in Fig. 5. A liquid-xenon jet was injected into vacuum through a tapered glass-capillary nozzle with a 20-μm diameter orifice. The plasma-generating laser was a 20-Hz repetition-rate, λ = 1064 nm Nd:YAG laser (Quantel Brilliant) generating 5-ns-long pulses of 350 mJ that were attenuated by a variable diffractive attenuator to 30 mJ. The pulses were focused onto the jet to a FWHM of ~10 μm. The laser-focus position could be manually shifted in the several-micrometers range among four discrete positions in the x–y plane and the jet position between two corresponding positions in the x direction. The plasma was imaged, in the direction illustrated in Fig. 5, with an EUV camera

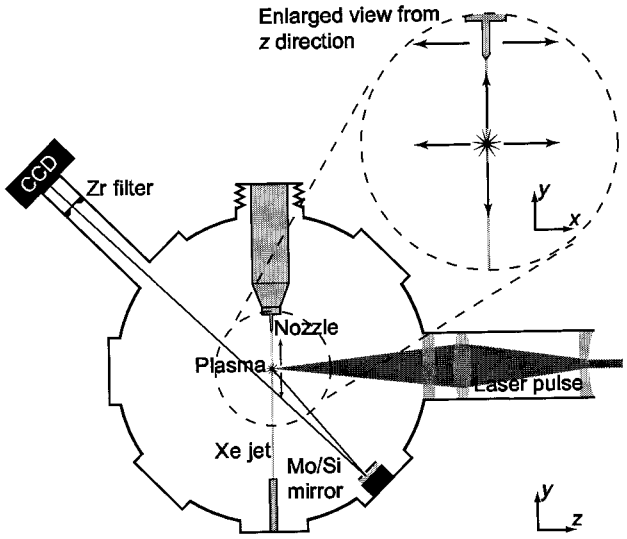

Fig. 5. Experimental arrangement illustrating how the xenon jet can be moved in the x direction and the laser focus moved in both the x and the y directions.

based on a spherical Mo–Si multilayer mirror, a cooled, thinned, backilluminated 1024 × 1024 pixel CCD array (Andor DO434), and thin Zr filters (<1 μm) to block non-EUV light. The camera has a resolution of ≈8 μm and is further described in Ref. 10. The pulse-to-pulse absolute in-band EUV flux was monitored by a flying-circus tool.[15]

Figure 2 is an image of a plasma from a single laser pulse. The FWHM of the plasma is ~26 μm. The laser-to-EUV conversion efficiency was 0.26%/(2%BW 2πsr) at λ = 13.45 nm.

To increase the integrated brightness uniformity we moved the plasma to four positions at the edges of a square in the x–y plane during one CCD acquisition. Twenty-five pulses were generated in each position, and the integrated emission profile is shown in Fig. 6. The brightness uniformity within an 18.2 μm × 18.2 μm square is ±5%, and the energy within the square is 15.0% of the total. To achieve the same uniformity within an 18.2 μm × 18.2 μm square with a Gaussian-shaped plasma, the FWHM of the plasma would have to be 66.0 μm, and only 6.4% of the total energy would be within the 18.2 μm × 18.2 μm square. Although the 2.3× gain is less than the theoretical value of 5.2× shown above, the experiment demonstrates the principle. The discrepancy from the theoretical value is due to instability of both position and energy of the individual pulses as well as to the nonsymmetrical shape of a single plasma imaged at 45° to the axis of symmetry (cf. Fig. 2).

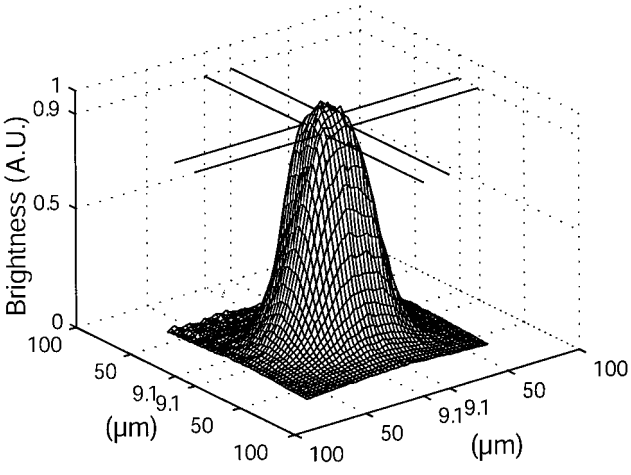

Fig. 6. Experimental result, illustrating the integrated EUV emission distribution of a 26-μm plasma scanned in four positions.

4. Conclusions

In the present paper we have shown how a scanned, small, high-brightness laser-plasma source can minimize photon losses while object illumination uniformity is maintained in small-field EUV and soft-x-ray imaging systems. Based on the specifications of the AIM tool, it has been calculated that the collection efficiency from a scanned liquid-jet laser-plasma source can be >5× higher than that of a static laser plasma and more than 2 orders of magnitude higher than that of a gas-discharge plasma. Experimentally, >2.3× better collection efficiency is demonstrated for a scanned laser-plasma than the theoretical value for a static single plasma. Increasing the collection efficiency means that lower-power sources can be applied. This has several advantages although the source in itself is not necessarily less expensive because of the assumed lower cost of discharge plasmas compared with that of laser plasmas. However, the major problem with prolonged operation of compact sources is the optics contamination induced by the source. This should scale with the total power of the source, strongly motivating the search for a low-power source. Also, thermal effects that may be detrimental to system operation will scale with the total power. Finally, one should note that, although the examples of this paper are based on the AIM tool requirement, the method should be generally applicable. However, a larger field might require scanning over more than four points, but this should actually increase the collection efficiency.

The authors gratefully acknowledge discussions and cooperation with all the staff of the no-longer-existing company Innolite.

References

1. M. Berglund, L. Rymell, M. Peuker, T. Wilhein, and H. M. Hertz, "Compact water-window x-ray microscopy," J. Microsc. **197,** 268–273 (2000).
2. G. A. Johansson, A. Holmberg, H. M. Hertz, and M. Berglund, "Design and performance of a laser-plasma-based compact soft x-ray microscope," Rev. Sci. Instrum. **73,** 1193–1197 (2002).
3. W. P. Ballard, D. A. Tichenor, D. J. O'Connell, L. J. Bernardez II, R. E. Lafon, R. J. Anderson, A. H. Leung, K. A. Williams, S. J. Haney, Y. E. Perras, K. L. Jefferson, T. L. Porter, D. Knight, P. K. Barr, J. L. V. de Vreugde, R. H. Campiotti, M. D. Zimmerman, T. A. Johnson, L. E. Klebanoff, P. A. Grunow, S. Graham, Jr., D. A. Buchenauer, W. C. Replogle, T. G. Smith, J. B. Wronosky, J. R. Darnold, K. L. Blaedel, H. N. Chapman,

J. S. Taylor, L. C. Hale, G. E. Sommargren, E. M. Gullikson, P. P. Naulleau, K. A. Goldberg, S. H. Lee, H. Shields, R. J. S. Pierre, and S. Ponti, "System and process learning in a full-field, high-power EUVL alpha tool," in *Emerging Lithographic Technologies VII,* R. L. Engelstad, ed., Proc. SPIE **5037** 47–57 (2003).
4. D. Stark, K. Dean, P. Gabella, J. Meute, J. Cashmore, M. Whitfield, A. Brunton, P. Gruenewald, and M. Gower, "EUV microexposure tool update," presented at the *1st International EUV Lithography Symposium,* Dallas, Tex., 15–17 October 2002; available at http://www.sematech.org.
5. A. Barty, J. S. Taylor, R. Hudyma, and E. Spiller, "Design and evaluation of system configurations for an EUV mask inspection microscope," Tech. Rep. UCRL-CR-149774 (Lawrence Livermore National Laboratory, Livermore, Calif., 2002); available at http://www.llnl.gov/library/.
6. Proceedings of the *EUVL Source Workshop,* Santa Clara, Calif., 23 February 2003; available at www.sematech.org.
7. I. V. Fomenkov, R. M. Ness, I. R. Oliver, S. T. Melnychuk, O. V. Khodykin, N. R. Bowering, C. L. Rettig, and J. R. Hoffman, "Performance and scaling of a dense plasma focus light source for EUV lithography," in *Emerging Lithographic Technologies VII,* R. L. Engelstad, ed., Proc. SPIE **5037,** 807–821 (2003).
8. U. Stamm, I. Ahmad, I. Balogh, H. Birner, D. Bolshukhin, J. Brudermann, S. Enke, F. Flohrer, K. Gbel, S. Gtze, G. Hergenhan, J. Kleinschmidt, D. Klpfel, V. Korobotchko, J. Ringling, G. Schriever, C. D. Tran, and C. Ziener, "High-power EUV lithography sources based on gas discharges and laser-produced plasmas," in *Emerging Lithographic Technologies VII,* R. L. Engelstad, ed., Proc. SPIE **5037,** 119–129 (2003).
9. G. D. Kubiak, L. Bernardez, and K. Krenz, "High-power extreme ultraviolet source based on gas jets," in *Emerging Lithographic Technologies II,* Y. Vladimirsky, ed., Proc. SPIE **3331,** 81–89 (1998).
10. B. A. M. Hansson, O. Hemberg, H. M. Hertz, M. Berglund, H.-J. Choi, B. Jacobsson, E. Janin, S. Mosesson, L. Rymell, J. Thoresen, and M. Wilner, "Characterization of a liquid-xenon-jet laser-plasma EUV source," Rev. Sci. Instrum. **75,** 2122–2129 (2004).
11. S. McNaught, "NGST/CEO presentation—Laser-produced plasma EUV source program," presented at the *EUV Source Workshop,* Santa Clara, Calif., 23 February 2003; available at http://www.sematech.org.
12. D. Rudolph, G. Schmahl, B. Niemann, M. Diehl, J. Thieme, T. Wilhein, C. David, and K. Michelmann, "Wet specimen imaging with an x-ray microscope with a pulsed plasma source," in *X-Ray Microscopy IV,* V. V. Aristov and A. I. Erko, eds. (Bogorodsjii Pechatnik, Chernogolovka, Moscow Region, Russia, 1994), pp. 381–386.
13. M. Antoni, W. Singer, J. Schultz, J. Wangler, I. Escudero-Sanz, and B. Kruizinga, "Illumination optics design for EUV lithography," in *Soft X-Ray and EUV Imaging Systems,* W. M. Kaiser and R. H. Stulen, eds., Proc. SPIE **4146,** 25–34 (2000).
14. H. N. Chapman and K. A. Nugent, "Illumination optics design for EUV lithography," in *Soft X-Ray and EUV Imaging Systems,* C. A. MacDonald, K. A. Goldberg, J. R. Maldonado, H. H. Chen-Mayer, and S. P. Vernon, eds., Proc. SPIE **3767,** 225–236 (1999).
15. B. A. M. Hansson, L. Rymell, M. Berglund, O. Hemberg, E. Janin, J. Thoresen, and H. M. Hertz, "Liquid-xenon-jet laser-plasma source for EUV lithography," in *Soft X-Ray and EUV Imaging Systems II,* D. A. Tichenor and J. A. Folta, eds., Proc. SPIE **4506,** 1–8 (2001).